frontiers in Oncology

ORIGINAL RESEARCH
published: 26 August 2021
doi: 10.3389/fonc.2021.741383

Facile Synthesis of Holmium-Based Nanoparticles as a CT and MRI Dual-Modal Imaging for Cancer Diagnosis

Tianqi Zhang[1], Mo Deng[2], Lei Zhang[3], Zerun Liu[4], Yang Liu[5], Shuyan Song[5], Tingting Gong[1] and Qinghai Yuan[1]**

[1] Department of Radiology, The Second Hospital of Jilin University, Changchun, China, [2] Department of Clinical Laboratory, The Second Hospital of Jilin University, Changchun, China, [3] Department of Neurology, The Second Hospital of Jilin University, Changchun, China, [4] Department of Clinical Pharmacy, Jilin University School of Pharmaceutical Science, Changchun, China, [5] State Key Laboratory of Rare Earth Resource Utilization, Changchun Institute of Applied Chemistry, Chinese Academy of Sciences, Changchun, China

OPEN ACCESS

Edited by:
Kelong Ai,
Central South University, China

Reviewed by:
Zhen Liu,
Beijing University of Chemical Technology, China
Yunlu Dai,
University of Macau, China

***Correspondence:**
Tingting Gong
gongtt01@jlu.edu.cn
Qinghai Yuan
yqh@jlu.edu.cn

Specialty section:
This article was submitted to Pharmacology of Anti-Cancer Drugs, a section of the journal Frontiers in Oncology

Received: *14 July 2021*
Accepted: *03 August 2021*
Published: *26 August 2021*

Citation:
Zhang T, Deng M, Zhang L, Liu Z, Liu Y, Song S, Gong T and Yuan Q (2021) Facile Synthesis of Holmium-Based Nanoparticles as a CT and MRI Dual-Modal Imaging for Cancer Diagnosis. Front. Oncol. 11:741383. doi: 10.3389/fonc.2021.741383

The rapid development of medical imaging has boosted the abilities of modern medicine. As single modality imaging limits complex cancer diagnostics, dual-modal imaging has come into the spotlight in clinical settings. The rare earth element Holmium (Ho) has intrinsic paramagnetism and great X-ray attenuation due to its high atomic number. These features endow Ho with good potential to be a nanoprobe in combined x-ray computed tomography (CT) and T_2-weighted magnetic resonance imaging (MRI). Herein, we present a facile strategy for preparing HoF_3 nanoparticles (HoF_3 NPs) with modification by PEG 4000. The functional PEG-HoF_3 NPs have good water solubility, low cytotoxicity, and biocompatibility as a dual-modal contrast agent. Currently, there is limited systematic and intensive investigation of Ho-based nanomaterials for dual-modal imaging. Our PEG-HoF_3 NPs provide a new direction to realize *in vitro* and *vivo* CT/MRI imaging, as well as validation of Ho-based nanomaterials will verify their potential for biomedical applications.

Keywords: nanomaterial, cancer, diagnosis, dual-model imaging, contrast agent

INTRODUCTION

Imaging technology plays an important role in modern medicine due to its ability to provide noninvasive but detailed information of anatomical structure and functional activities during the progress of a disease. However, single-model imaging methods cannot always meet the criteria for diagnosing co2mplex diseases (1, 2); thus, multi-modal imaging has become the new direction for imaging technology development (3–6). There are two main means to achieve multi-modal imaging (1): endow one device with multiple imaging capabilities; or (2) construct multi-modal contrast agents (CAs) for diagnosis. Conflicts between various methods and high costs have limited the feasibility of the first method. Hence, researchers are focusing their efforts on developing multi-modal CAs that can be widely used in magnetic resonance imaging (MRI), X-ray computed tomography (CT), as well as fluorescence imaging (FI) (7–13). Due to the penetrative limitation of FI *in vivo*, CT and MRI are more commonly applied for clinical diagnosis (14–17). CT is the most cost-effective examination and offers strong X-ray penetration, which has very high resolution for bone and calcification but poor resolution for soft tissue. Notably, MRI can remedy this

shortcoming. Therefore, the combination of CT and MRI can significantly improve diagnostic ability (2, 18–24).

At present, CT and MRI examinations are used independently in clinical settings. Small iodinated molecule nanomaterials are routinely applied as CT CAs to assist in disease diagnosis. Due to the lack of X-ray absorption, a very large amount of such CAs for intravenous injection is needed to meet the contrast requirement, usually 80-150 ml per adult for angiography (25, 26). Such a high dose is not only likely to cause allergy, but it can also lead to irreversible renal damage (27–29). Furthermore, as small molecular iodide is quickly excreted by the kidney, its short circulation lifetime can affect imaging quality for certain diseases. Similarly, MRI has its own limitations. Gd-chelates are the most commonly used commercial MRI CAs in clinical settings. However, Gd-based CAs can accumulate in the central nervous system and lead to renal fibrosis (30). Another notable disadvantage of MRI is that the optimum magnetic field strength for current Gd-based CAs is less than 1.0 T (31), whereas the trend in clinical MRI is to use ultra-high magnetic fields of 7.0 T or even higher because of the better imaging quality (32). 7.0 T MRI has been available in the market since 2017, and ultra-high field strength MRI equipment will become mainstream in the future. As a result, several researchers have been focusing on developing new CAs to suit this powerful visualization tool. Tb, Ho, and Dy are the elements with the largest magnetic moments in the periodic table and can cause considerable transverse relaxation of hydrogen protons in free water. Thus, Tb, Ho, and Dy-based materials are the best choices for ultra-high field T_2 CAs (33–36). Against the background of continuous pursuit of ultra-high field intensity MRI, research on MRI CAs based on large magnetic moment elements is likely to experience rapid growth in the near future. Thus, we developed a facile strategy to construct control-sized PEGylated HoF_3 nanoparticles (PEG-HoF_3 NPs) as a dual-modal imaging CA. **Scheme 1**. illustrates the design of our study. We used a facile one-pot solvothermal approach to obtain Ho-based nanomaterial, which has a high X-ray attenuation and large magnetic moment. PEG-HoF_3 NPs offer great biocompatibility and low cytotoxicity due to the existence of poly(ethylene glycol) (PEG). As a result, these NPs could be used as CT/MRI dual-modal imaging CAs both *in vitro* and *in vivo*, confirming the potential of Ho-based nanomaterials for bioapplication research.

MATERIALS AND METHODS

Chemicals

$HoCl_3$•$6H_2O$, poly(ethylene glycol) (PEG, MW = 4000 Da) was obtained from Sigma-Aldrich. NH_4F and ethylene glycol (EG) were obtained from Beijing Chemicals. Dimethyl sulfoxide (DMSO) were obtained from Sigma-Aldrich. DMEM and FBS were purchased from Gibco.

Preparation of PEG-HoF_3 NPs

PEG-HoF_3 NPs were fabricated *via* a one-pot solvothermal method. Firstly, 0.8 mmol $HoCl_3$•$6H_2O$ was dissolved in 5 mL

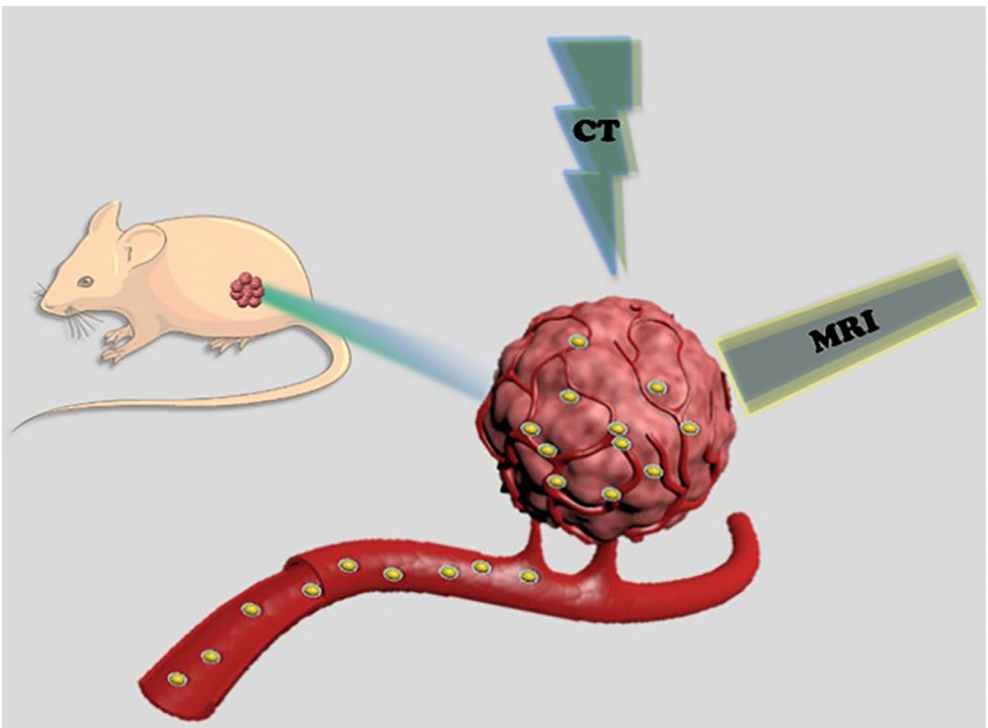

SCHEME 1 | Schematic illustration of PEG-HoF_3 NPs for enhanced CT and T_2-weighted duel-model imaging.

of EG to form a clear solution. Then, 0.6 g of PEG 4000 was added to 15 mL of EG to form a clear solution. Next, prepared EG with 2.4 mmol NH_4F added to the mixture of above two solutions. This mixed solutions were vigorously stirred for about 40 min and then transferred to a 50 mL Teflon-lined autoclave and kept at 200°C for 10 h. When the system was cooled down, all collected NPs were washed several times.

In Vitro Cytotoxicity Assessment

Human cervix cancer cells (HeLa) and mouse fibroblast cells (L929) were cultured in DMEM with 10% FBS, 1% penicillin, and 1% streptomycin at a 37°C in a 5% CO_2 incubator. After incubation in 96-well cell culture plates for 24 h, different concentrations of PEG-HoF_3 NPs (0, 25, 50, 100, 200, 300 μg/mL) were added to the HeLa cells and L929 cells and incubated for another 24 h. Next, 10 μL (5 mg/mL) MTT was added to 96-well cell culture plates and kept for an additional 4 h at 37°C. Finally, the medium was removed and DMSO was added for 15 min to dissolve the formazan. The absorbance peak at 570 nm was measured by a microplate reader.

Histological and Hematology Assessment

Kunming mice (18-25 g) were obtained from the Center for Experimental Animals, Jilin University (Changchun, China). All operations are carried out in accordance with relevant national regulations. For histological assessment, 100 μL PEG-HoF_3 NPs (300 μg/mL) and 100 μL 0.9% NaCl solution were administered to Kunming mice *via* tail vein. After 30 days, Major organs and tissues (heart, liver, spleen, lung, kidney, and muscle) were collected. All tissues samples were formalin-fixed, paraffin-embedded, and stained with H&E. Tissue sections were observed under an optical microscope (×10). Blood samples were also obtained from the PEG-HoF_3 NPs and NaCl injected mouse groups for routine blood testing and biochemical indices testing.

CT Imaging

Different concentration of PEG-HoF_3 NPs and Iohexol aqueous solutions (I or Ho 0, 0.25, 0.5, 1, 2, 4 mmol/mL) were prepared for *in vitro* CT imaging. When the suitable con-centration was determined, *in vivo* CT images were obtained on Kunming mice. After intraperitoneal anesthesia with chloral hydrate, 100 μL PEG-HoF_3 NPs (2 mg/mL) were injected into these mice *via* tail vein and images were obtained at different times (0, 1, 2, 6, 12, 24 h). CT was performed using a clinical CT scanner, and the parameters were tube voltage of 120 kVp, tube current of 300 mAs, 0.9 mm thickness, 0.99 pitch, window width of 200 HU, and window level of 45 HU.

T_2-Weighted MRI

Different concentrations of PEG-HoF_3 NPs aqueous solutions (Ho 0, 0.0625, 0.125, 0.25, 0.5, 1 mmol/mL) were prepared for *in vitro* T_2-weighted MRI. Preliminary preparation was similar to the above steps. MRI was performed on a clinical MR scanner. 100 uL PEG-HoF_3 NPs (0.8 mg/mL) were injected into mice as above. These mice were scanned pre-injection and 1, 2, 4, 12, and 24 h post-injection. The MR scanner parameters were TR=7279.7 ms, TE=113 ms and FOV=240x240 mm.

RESULTS AND DISCUSSION

Preparation and Characterization of PEG-HoF_3 NPs

Uniform HoF_3 NPs were prepared through a one-pot solvothermal method using PEG 4000 as a surfactant, as illustrated in **Figure 1A**. The TEM images demonstrate the good dispersivity of PEG-HoF_3 NPs, and the existence of Ho and F element is proved by HADDF-STEM image and EDS mapping (**Figures 1B–F**), and the high-resolution TEM image shows that the width of lattice fringes about PEG-HoF_3 NPs was 0.3401 nm. The SEM image shows the spherical nanoparticles with an average diameter of 38 nm; the diameter of PEG-HoF_3 NPs was normally distributed in the range of 30–55 nm (**Figure S1**). In order to ascertain the hydrodynamic diameters of PEG-HoF_3 NPs, the dynamic light scattering (DLS) was performed, and the results show the average hydrodynamic diameter are suitable for using in organism in different solvents (**Figure 2A**). Meanwhile, the Zeta potential of PEG-HoF_3 NPs was 5.83 mV with the decoration of PEG. These value are suitable for nanomaterial which will be applied *in vivo*. XRD analysis exhibited several strong peaks, which indicated the highly crystalline nanostructure of this material. The diffraction peaks of the nanoparticles can be indexed to orthorhombic HoF_3, which matches the card (PDF 00-023-0284) in **Figure 2B** (34). XPS spectra verified that the NPs contained Ho 4d, F 1s (**Figures 2C, D**), further confirming the existence of HoF_3 NPs. The peaks of C and O confirmed the presence of PEG (**Figure S2**). The peak in 3391 cm^{-1} of FTIR spectrum further confirm the existence of PEG (**Figure S3**). Due to the low toxicity and bio-tolerability of PEG, it was approved for use in biopharmaceuticals by the US FDA several years ago (37, 38). Using PEG 4000 to modify the surface of HoF_3 NPs not only reduced cytotoxicity, but also enhanced dispersibility in water and phosphate-buffered saline (PBS) solution. The picture shows good stability of PEG-HoF_3 NPs in normal saline and PBS solution (**Figure S4**). There was no obvious Ho^{3+} ion dissociation after long-term dialysis in PBS solution (pH=7.4) with PEG-HoF_3 NPs.

Biocompatibility Assessment of PEG-HoF_3 NPs

Biocompatibility assessment should be carried out before nanomaterial imaging probes are applied *in vivo*. Due to the lack of data about the application of Ho-based nanomaterial *in vivo*, we carried out a variety of tests to assess the safety of PEG-HoF_3 NPs. The cytotoxicity of PEG-HoF_3 NPs was evaluated by the MTT cell proliferation assay. We chose HeLa and L929 cells to evaluate the toxicity of the new Ho-based nanomaterial by observing damage in cancer cells and normal cells, respectively. The cell viability results are depicted in **Figures 3A, B**. The two cell types were exposed to PEG-HoF_3 NPs at different extracellular

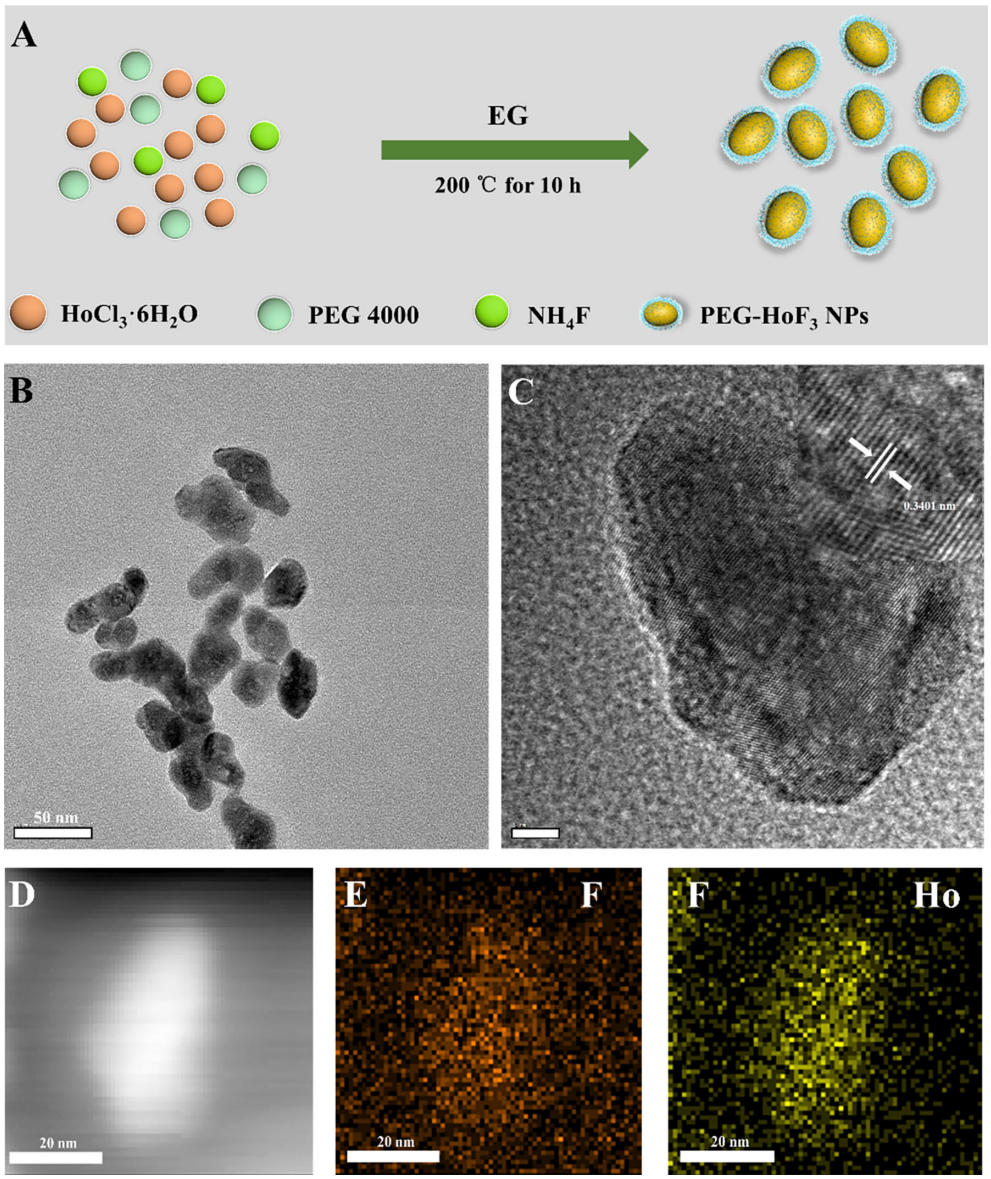

FIGURE 1 | **(A)** The synthetic process of PEG-HoF_3 NPs; **(B, C)** TEM image of PEG-HoF_3 NPs, the particles size is about 30-40nm and its lattice fringes; **(D–F)**. HADDF-STEM image of PEG-HoF_3 and EDS mapping of F, Ho element.

concentrations (0-300 μg/mL). As expected, the new PEGylated Ho-based nanoparticles had great biocompatibility. Cell viability was still about 85% of the highest concentration (300 μg/mL) in both cell strains. We further investigated histological damage caused by PEG-HoF_3 NPs through long-term toxicity assessment. Thirty days after injection, the two groups' mice were sacrificed. The main organs and tissues (heart, liver, spleen, lung, kidney, and muscle) underwent H&E staining for histopathological assessment.

Paraffin sections conformed that there was no significant damage or severe inflammation in organs or tissues in either the control group or PEG-HoF_3 NPs injection group (**Figure 3C**). Encouraged by these results, quantitative analysis of PEG-HoF_3 NPs potential toxicity was carried out *via* blood testing and biochemical examination. Routine blood tests can be used to observe changes in the distribution of blood cells to judge the condition of mice, and biochemical examination can be used to detect various products of metabolism in blood to show the condition of organs such as liver or kidney. Thirty days after injection, there were no significant abnormalities in the morphology or indices of blood cells **Figure 4**. Metabolism of the main organs also remained stable, which was consistent with the physiological status of the mice. Taken together, the results confirmed that Ho-based nanomaterials offer great potential for bio-application researches due to their high biocompatibility.

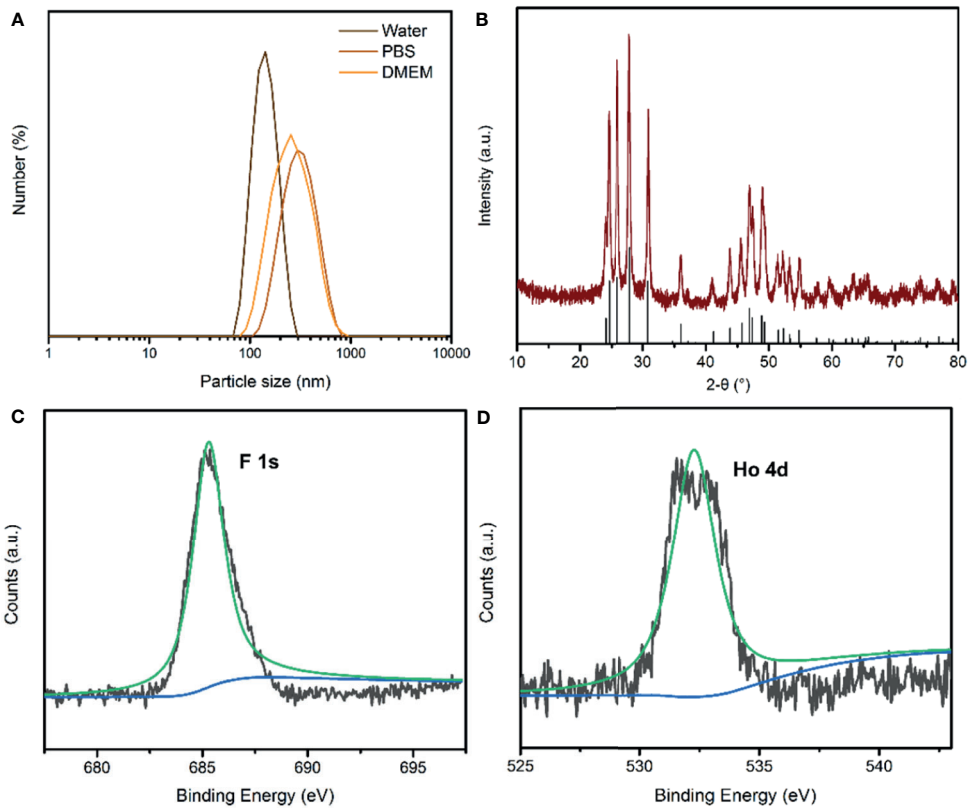

FIGURE 2 | **(A)** The dynamic light scattering (DLS) of PEG-HoF_3 NPs; **(B)** XRD pattern of PEG-HoF_3 NPs; **(C, D)** Higher-resolution XPS spectra of Ho 4d and F1s, respectively.

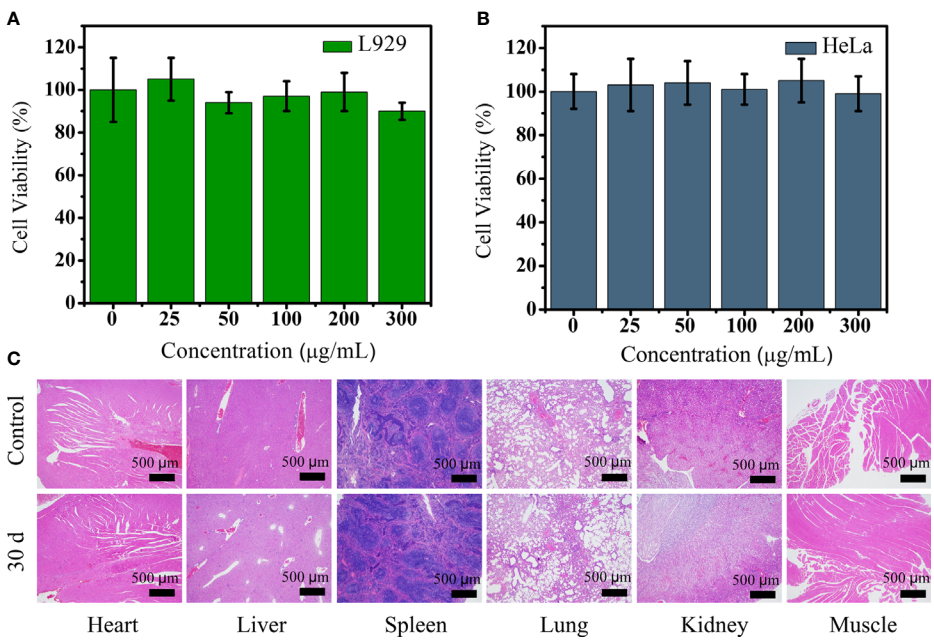

FIGURE 3 | **(A, B)** Viability of L929 and HeLa cells after incubation with different concentrations of PEG-HoF_3 NPs; **(C)** Tissue sections of 6 major organs from mouse which injected with PEG-HoF_3 NPs *via* tail vein.

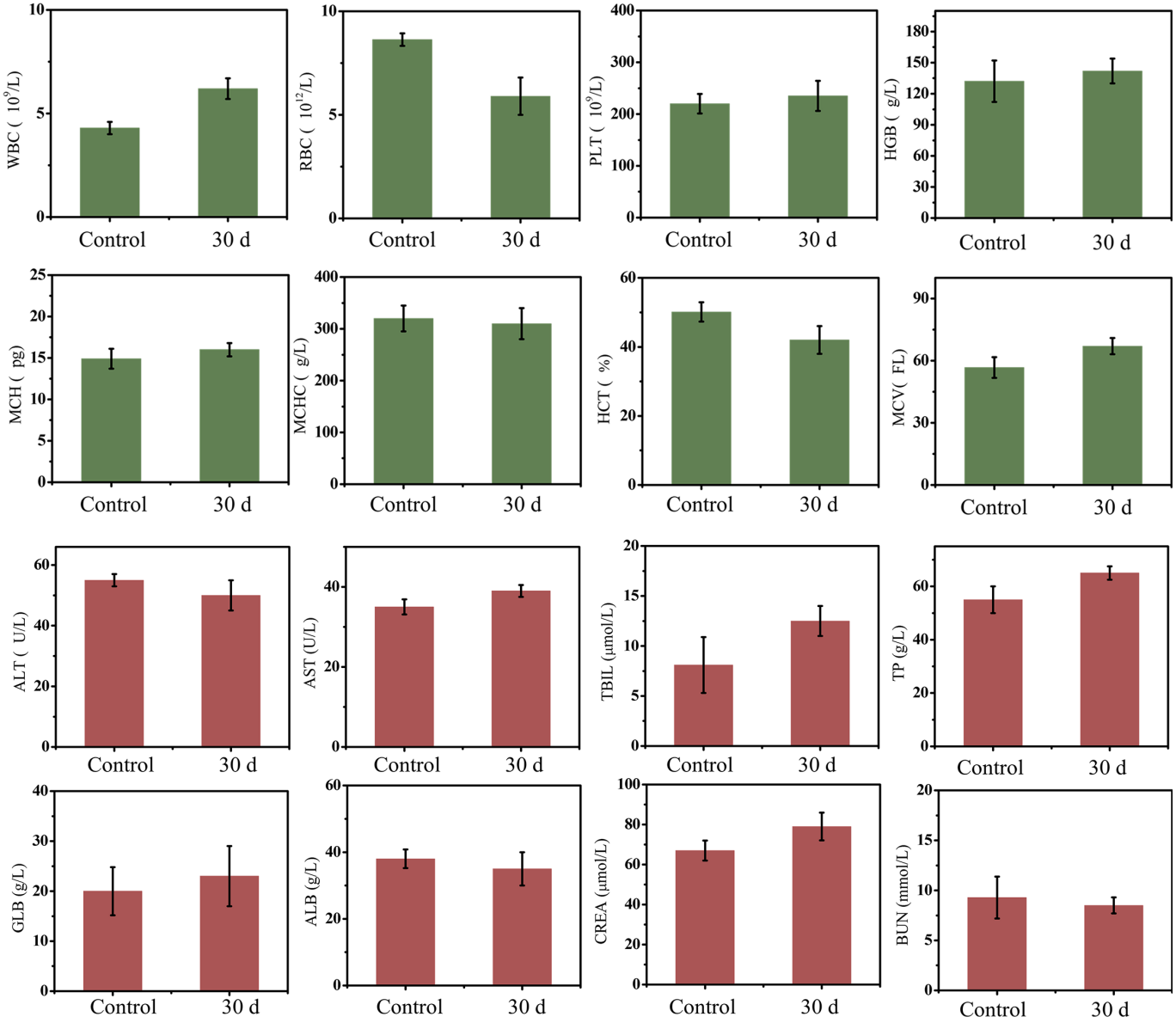

FIGURE 4 | Mice blood testing and biochemical examination, there is no evitable changes in two groups.

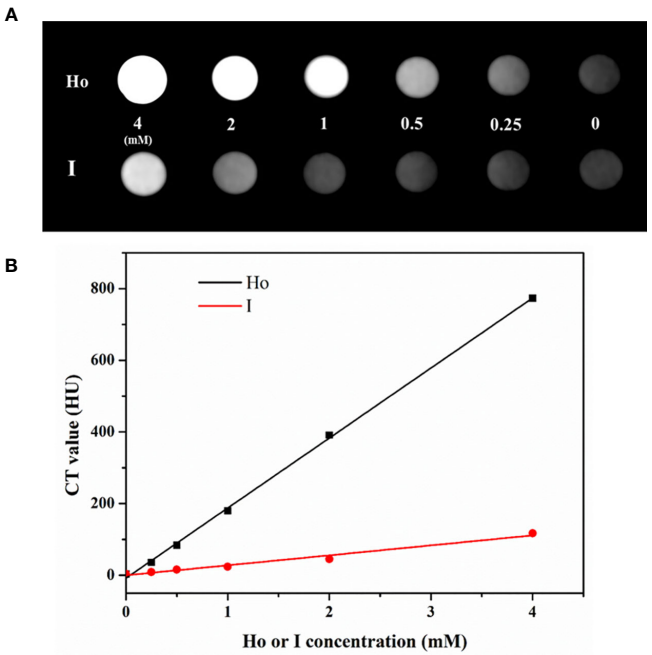

FIGURE 5 | **(A)** *In vitro* CT images of PEG-HoF_3 NPs and Iohexol aqueous solution with different concentration; **(B)** CT value of corresponding tube of A.

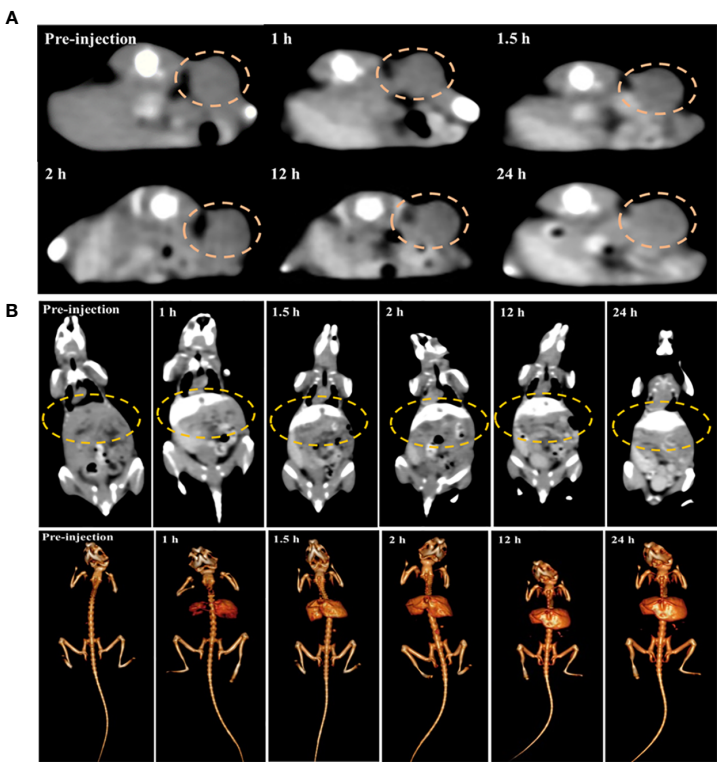

FIGURE 6 | **(A, B)** Changes of tumor site and mouse liver in different time point before versus post-injection of PEG-HoF_3 NPs.

CT Imaging

As a rare earth element, Ho has an atomic number of 67, which is much higher than iodine's atomic number of 53. The inherent characteristics of Ho, specifically its high x-ray attenuation, result in the significantly improved imaging ability of Ho-based CAs in CT. The *in vitro* CT imaging results are shown in **Figure 5A**. Different concentrations of PEG-HoF_3 NPs and Iohexol aqueous solution (0-4 mM) were prepared in Eppendorf tubes and the solutions became brighter as the concentration increased. As shown in **Figure 5B**, the Hounsfield Units (HU) value of PEG-HoF_3 NPs was significantly higher than that of iodine-based CAs, as we expected, and the HU values for both increased linearly. Therefore, the necessary dose of PEG-HoF_3 NPs is much lower than that of iodine-based CAs to achieve the same contrast effect *in vivo*, which may reduce the risks of large doses of CAs (39).

After cytotoxicity assessment of PEG-HoF_3 NPs, tumor-bearing Kunming mice were selected to test the CT contrast effect *in vivo*. The distribution of PEG-HoF_3 NPs was monitored by a CT scanner at different time points. We then compared the images at these time points with the images pre-injection: the brightness of the tumor site was obviously higher after 24 h (**Figure 6A**).

We also tracked the brightness of the liver and kidney after administering PEG-HoF_3 NPs *via* the tail vein (**Figures 6B** and **S5**). Usually, small molecule iodine CAs are not long-lasting in the liver, which decreases the diagnostic ability of liver disease to some extent. However, as shown in **Figure S5**, the liver of the

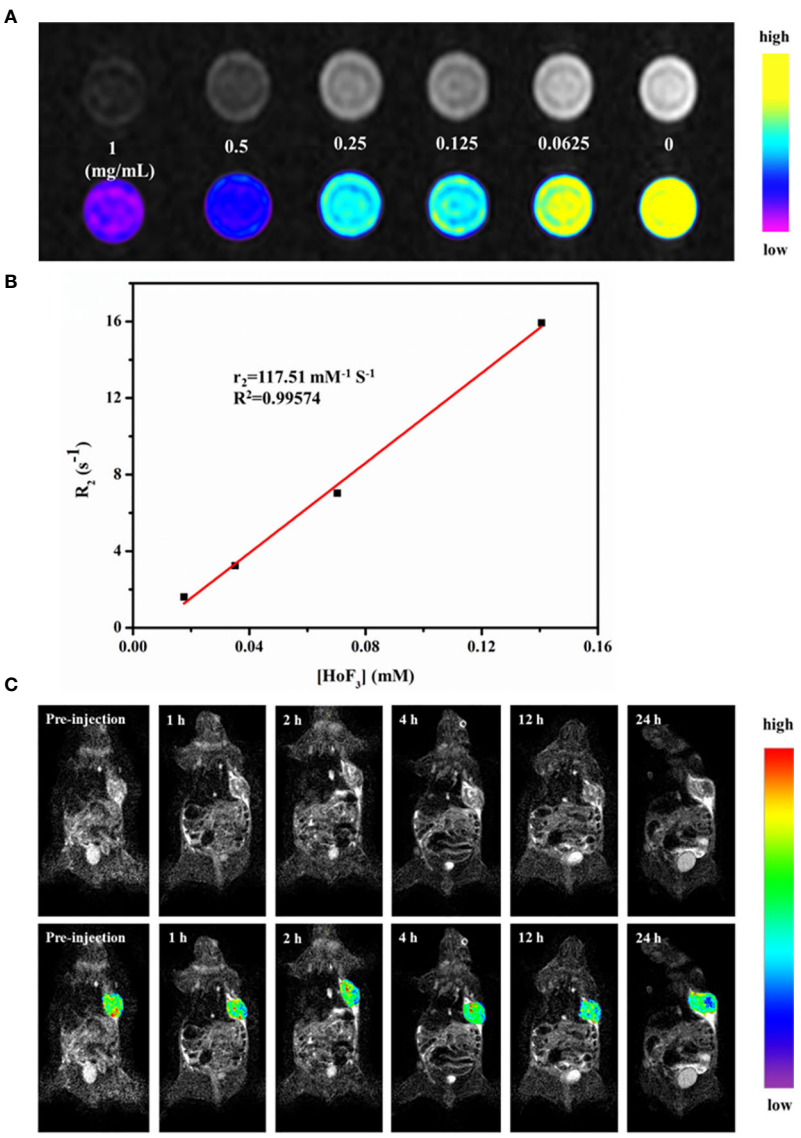

FIGURE 7 | **(A)** *In vitro* T_2-weighted MRI images of PEG-HoF_3 NPs with different concentration; **(B)** The r_2 relaxivity plot of PEG-HoF_3 NPs; **(C)** Signal changes of tumor site in different time point before and post-injection of PEG-HoF_3 NPs.

mice maintained a high contrast effect after 24 h, which likely indicates the uptake of PEG-HoF_3 NPs by hepatocytes. However, there was no obvious enhancement in the kidney at the time points we used. This may indicate that the uptake of PEG-HoF_3 NPs by renal cells is limited and that the size and shape of PEG-HoF_3 NPs prevented its filtration through the kidney. It is possible that the above mechanism can decrease the side effects of CAs on the kidney, and warrants further study.

T_2-Weighted MRI

To date, there have been few studies on Ho-based MRI imaging. It has been confirmed that Ho-based nanomaterial has T_2-weighted MRI contrast ability owing to its intrinsic paramagnetism. However, the magnetic resonance relaxivity of NPs can differ due to their size, form, and even synthesis methods. For this reason, we firstly validated the feasibility of PEG-HoF_3 NPs as a T_2-weighted MRI CAs *in vitro*. Different concentrations of PEG-HoF_3 NPs aqueous solution were tested on a clinical MR scanner. T_2-weighted images of PEG-HoF_3 NPs aqueous solution (0-1 mg/mL) gradually darkened with an increasing Ho concentration (**Figure 7A**). According to the concentration of PEG-HoF_3 NPs, the r_2 relaxivity value of this new contrast agent is 117.51 mM^{-1} S^{-1} (**Figure 7B**). Next, we further explored the potential of PEG-HoF_3 NPs as negative MRI CAs in tumor-bearing mice. T_2-weighted MRI was performed on the same scanner at different times (1, 2, 4, 12, 24 h) after intravenous injection of PEG-HoF_3 NPs (**Figure 7C**). The results showed no significant changes in the signal of the tumor site within 0 to 2 h. However, after 12 h, the signal of the tumor site decreased significantly and a large dark area gradually presented. At 24 h, the negative contrast agent filled the center of tumor site. These results also confirm long term circulation of PEG-HoF_3 NPs, which will be helpful for improving the detection of tumors at specific places.

CONCLUSIONS

We firstly synthesized a new Ho-based NP *via* a one-pot solvothermal method. The new PEG-HoF_3 NPs had a uniform size and showed good dispersibility in aqueous solution. Cytotoxicity assessment and histological analysis indicated that the new Ho-based NPs had good biocompatibility and low toxicity for applications *in vivo*. We then further verified the imaging ability of the PEG-HoF_3 NPs *in vitro* and *vivo*. The results showed that PEG-HoF_3 NPs had an excellent contrast effect in both CT and T_2-weighted MRI. Based on this desirable performance, we expect that PEG-HoF_3 NPs hold great promise for dual-modal imaging and that Ho-based nanomaterials warrant further research.

DATA AVAILABILITY STATEMENT

The original contributions presented in the study are included in the article/**Supplementary Material**. Further inquiries can be directed to the corresponding authors.

ETHICS STATEMENT

The animal study was reviewed and approved by Laboratory Animal Center of Jilin University.

AUTHOR CONTRIBUTIONS

TZ contributed to conception and design of the study. MD and LZ provided the database of mice. ZL contributed to the data of revised manuscript. YL and SS provided the testing instrument and site. TZ wrote the first draft of the manuscript. TG and QY revised and edited the manuscript. All authors contributed to the article and approved the submitted version.

FUNDING

This work was supported by the Program of Science and Technology Development Plan of Jilin Province of China (Nos. 20190201218JC), the Health Special Project of Jilin Province Department of Finance (Nos. 2019SCE7025, 2020SCZT088).

SUPPLEMENTARY MATERIAL

The Supplementary Material for this article can be found online at: https://www.frontiersin.org/articles/10.3389/fonc.2021.741383/full#supplementary-material.

REFERENCES

1. Shi J, Sun X, Zheng S, Li J, Fu X, Zhang H. A New Near-Infrared Persistent Luminescence Nanoparticle as a Multifunctional Nanoplatform for Multimodal Imaging and Cancer Therapy. *Biomaterials* (2018) 152:15–23. doi: 10.1016/j.biomaterials.2017.10.032
2. Padmanabhan P, Kumar A, Kumar S, Chaudhary RK, Gulyas B. Nanoparticles in Practice for Molecular-Imaging Applications: An Overview. *Acta Biomater* (2016) 41:1–16. doi: 10.1016/j.actbio.2016.06.003
3. Chen C, Liu J, Chen Y, Li C, Liu X, Huang H, et al. Sub-10 Nm Sr2LuF7:Yb/Er@Sr2GdF7@SrF2 Up-Conversion Nanocrystals for Up-Conversion Luminescence-Magnetic Resonance-Computed Tomography Trimodal Bioimaging. *ACS Appl Mater Interfaces* (2017) 9(7):5748–56. doi: 10.1021/acsami.6b14007
4. Jin L, Liu J, Tang Y, Cao L, Zhang T, Yuan Q, et al. MnO2-Functionalized Co-P Nanocomposite: A New Theranostic Agent for pH-Triggered T1/T2 Dual-Modality Magnetic Resonance Imaging-Guided Chemo-Photothermal Synergistic Therapy. *ACS Appl Mater Interfaces* (2017) 9(48):41648–58. doi: 10.1021/acsami.7b10608
5. Li Q, Li X, Zhang L, Zuo J, Zhang Y, Liu X, et al. An 800 Nm Driven NaErF4@NaLuF4 Upconversion Platform for Multimodality Imaging and Photodynamic Therapy. *Nanoscale* (2018) 10(26):12356–63. doi: 10.1039/c8nr00446c
6. Ma S, Zhang J, Xia S, Yin W, Qin Y, Lei R, et al. Three-Dimensional Angiography Fused With CT/MRI for Multimodal Imaging of Nanoparticles Based on Ba4Yb3F17:Lu(3+),Gd(3+). *Nanoscale* (2018) 10(28):13402–9. doi: 10.1039/c8nr03054e
7. van Schooneveld MM, Cormode DP, Koole R, van Wijngaarden JT, Calcagno C, Skajaa T, et al. A Fluorescent, Paramagnetic and PEGylated Gold/Silica

Nanoparticle for MRI, CT and Fluorescence Imaging. *Contrast Media Mol Imaging* (2010) 5(4):231–6. doi: 10.1002/cmmi.376
8. Curcio A, Silva AKA, Cabana S, Espinosa A, Baptiste B, Menguy N, et al. Iron Oxide Nanoflowers @ CuS Hybrids for Cancer Tri-Therapy: Interplay of Photothermal Therapy, Magnetic Hyperthermia and Photodynamic Therapy. *Theranostics* (2019) 9(5):1288–302. doi: 10.7150/thno.30238
9. Zhang X, Xi ZQ, Machuki JO, Luo JJ, Yang DZ, Li JJ, et al. Gold Cube-In-Cube Based Oxygen Nanogenerator: A Theranostic Nanoplatform for Modulating Tumor Microenvironment for Precise Chemo-Phototherapy and Multimodal Imaging. *ACS Nano* (2019) 13(5):5306–25. doi: 10.1021/acsnano.8b09786
10. Wang ZX, Wu LM, Chen M, Zhou SX. Facile Synthesis of Superparamagnetic Fluorescent Fe3O4/ZnS Hollow Nanospheres. *J Am Chem Soc* (2009) 131 (32):11276–+. doi: 10.1021/ja903246e
11. Jeffrey RB. Imaging Pancreatic Cysts With CT and MRI. *Digest Dis Sci* (2017) 62(7):1787–95. doi: 10.1007/s10620-017-4501-6
12. Schieda N, Lim RS, McInnes MDF, Thomassin I, Renard-Penna R, Tavolaro S, et al. Characterization of Small (<4cm) Solid Renal Masses by Computed Tomography and Magnetic Resonance Imaging: Current Evidence and Further Development. *Diagn Intervent Imaging* (2018) 99(7-8):443–55. doi: 10.1016/j.diii.2018.03.004
13. Ahlawat S, Baig A, Blakeley JO, Jacobs MA, Fayad LM. Multiparametric Whole-Body Anatomic, Functional, and Metabolic Imaging Characteristics of Peripheral Lesions in Patients With Schwannomatosis. *J Magnet Resonance Imaging: JMRI* (2016) 44(4):794–803. doi: 10.1002/jmri.25236
14. Shan X, Chen Q, Yin X, Jiang C, Li T, Wei S, et al. Polypyrrole-Based Double Rare Earth Hybrid Nanoparticles for Multimodal Imaging and Photothermal Therapy. *J Mater Chem B* (2020) 8(3):426–37. doi: 10.1039/c9tb02254f
15. Lyu M, Zhu DM, Duo YH, Li Y, Quan H. Bimetallic Nanodots for Tri-Modal CT/MRI/PA Imaging and Hypoxia-Resistant Thermoradiotherapy in the NIR-II Biological Windows. *Biomaterials* (2020) 233:119656. doi: 10.1016/j.biomaterials.2019.119656
16. Li Z, Guan M, Sun D, Xu Y, Li F, Xiong W. A Novel MRI- and CT-Based Scoring System to Differentiate Malignant From Osteoporotic Vertebral Fractures in Chinese Patients. *BMC Musculoskelet Disord* (2018) 19(1):406. doi: 10.1186/s12891-018-2331-0
17. Jin X, Fang F, Liu J, Jiang C, Han X, Song Z, et al. An Ultrasmall and Metabolizable PEGylated NaGdF4:Dy Nanoprobe for High-Performance T (1)/T(2)-Weighted MR and CT Multimodal Imaging. *Nanoscale* (2015) 7 (38):15680–8. doi: 10.1039/c5nr04065e
18. Park EA, Lee W, Kang DK, Kim SJ, Kim YJ, Kim Y, et al. Comparison of Iohexol-380 and Iohexol-350 for Coronary CT Angiography: A Multicenter, Randomized, Double-Blind Phase 3 Trial. *Korean J Radiol* (2016) 17(3):330–8. doi: 10.3348/kjr.2016.17.3.330
19. Bolen MA, Brinza E, Renapurkar RD, Kim ESH, Gornik HL. Screening CT Angiography of the Aorta, Visceral Branch Vessels, and Pelvic Arteries in Fibromuscular Dysplasia. *JACC Cardiovasc Imaging* (2017) 10(5):554–61. doi: 10.1016/j.jcmg.2016.04.010
20. Nijssen EC, Rennenberg RJ, Nelemans PJ, Essers BA, Janssen MM, Vermeeren MA, et al. Prophylactic Hydration to Protect Renal Function From Intravascular Iodinated Contrast Material in Patients at High Risk of Contrast-Induced Nephropathy (AMACING): A Prospective, Randomised, Phase 3, Controlled, Open-Label, Non-Inferiority Trial. *Lancet* (2017) 389 (10076):1312–22. doi: 10.1016/S0140-6736(17)30057-0
21. Wang Z, Jia T, Sun QQ, Kuang Y, Liu B, Xu MS, et al. Construction of Bi/phthalocyanine Manganese Nanocomposite for Trimodal Imaging Directed Photodynamic and Photothermal Therapy Mediated by 808 Nm Light. *Biomaterials* (2020) 228:119569. doi: 10.1016/j.biomaterials.2019.119569
22. Ai K, Huang J, Xiao Z, Yang Y, Bai Y, Peng J. Localized Surface Plasmon Resonance Properties and Biomedical Applications of Copper Selenide Nanomaterials. *Mater Today Chem* (2021) 20:100402. doi: 10.1016/j.mtchem.2020.100402
23. Wang J, Sui L, Huang J, Miao L, Nie Y, Wang K, et al. MoS2-Based Nanocomposites for Cancer Diagnosis and Therapy. *Bioactive Mater* (2021) 6(11):4209–42. doi: 10.1016/j.bioactmat.2021.04.021
24. Huang Q, Wu W, Ai K, Liu J. Highly Sensitive Polydiacetylene Ensembles for Biosensing and Bioimaging. *Front Chem* (2020) 8:565782. doi: 10.3389/fchem.2020.565782
25. Estelrich J, Sanchez-Martin MJ, Busquets MA. Nanoparticles in Magnetic Resonance Imaging: From Simple to Dual Contrast Agents. *Int J Nanomed* (2015) 10:1727–41. doi: 10.2147/IJN.S76501
26. Rohrer M, Bauer H, Mintorovitch J, Requardt M, Weinmann HJ. Comparison of Magnetic Properties of MRI Contrast Media Solutions at Different Magnetic Field Strengths. *Invest Radiol* (2005) 40(11):715–24. doi: 10.1097/01.rli.0000184756.66360.d3
27. Kraff O, Quick HH. 7t: Physics, Safety, and Potential Clinical Applications. *J Magnet Resonance Imaging: JMRI* (2017) 46(6):1573–89. doi: 10.1002/jmri.25723
28. Chen L, Huang Q, Zhao T, Sui L, Wang S, Xiao Z, et al. Nanotherapies for Sepsis by Regulating Inflammatory Signals and Reactive Oxygen and Nitrogen Species: New Insight for Treating COVID-19. *Redox Biol* (2021) 45:102046. doi: 10.1016/j.redox.2021.102046
29. Sui L, Wang J, Xiao Z, Yang Y, Yang Z, Ai K. ROS-Scavenging Nanomaterials to Treat Periodontitis. *Front Chem* (2020) 8:595530. doi: 10.3389/fchem.2020.595530
30. Ni D, Zhang J, Bu W, Zhang C, Yao Z, Xing H, et al. PEGylated NaHoF4 Nanoparticles as Contrast Agents for Both X-Ray Computed Tomography and Ultra-High Field Magnetic Resonance Imaging. *Biomaterials* (2016) 76:218–25. doi: 10.1016/j.biomaterials.2015.10.063
31. Gonzalez-Mancebo D, Becerro AI, Rojas TC, Garcia-Martin ML, de la Fuente JM, Ocana M. HoF3 and DyF3 Nanoparticles as Contrast Agents for High-Field Magnetic Resonance Imaging. *Part Part Syst Char* (2017) 34(10): 1700116. doi: 10.1002/Ppsc.201700116
32. Das GK, Johnson NJ, Cramen J, Blasiak B, Latta P, Tomanek B, et al. NaDyF4 Nanoparticles as T2 Contrast Agents for Ultrahigh Field Magnetic Resonance Imaging. *J Phys Chem Lett* (2012) 3(4):524–9. doi: 10.1021/jz201664h
33. Marasini S, Yue H, Ho SL, Jung KH, Park JA, Cha H, et al. D-Glucuronic Acid-Coated Ultrasmall Paramagnetic Ln(2)O(3) (Ln = Tb, Dy, and Ho) Nanoparticles: Magnetic Properties, Water Proton Relaxivities, and Fluorescence Properties. *Eur J Inorg Chem* (2019) 2019(34):3832–9. doi: 10.1002/ejic.201900378
34. D'Souza AA, Shegokar R. Polyethylene Glycol (PEG): A Versatile Polymer for Pharmaceutical Applications. *Expert Opin Drug Deliv* (2016) 13(9):1257–75. doi: 10.1080/17425247.2016.1182485
35. Ai K, Liu Y, Liu J, Yuan Q, He Y, Lu L. Large-Scale Synthesis of Bi(2)S(3) Nanodots as a Contrast Agent for *In Vivo* X-Ray Computed Tomography Imaging. *Adv Mater* (2011) 23(42):4886–91. doi: 10.1002/adma.201103289
36. Liu JH, Wang L, Zhang TQ, Wang JQ, Gong X, Cui FZ, et al. Facile Synthesis of Biocompatible Fe3O4-Based Nanoparticles for pH-Responsive Dual-Model Magnetic Resonance Imaging- Guided Tumour Eradication by Photothermal Therapy. *Chin J Anal Chem* (2019) 47(5):678–85. doi: 10.1016/S1872-2040(19)61158-8
37. Zhang TQ, Han XL, He YY, He XJ, Wang JQ, Yuan QH, et al. Facile Synthesis of PEGylated Tungsten-Based Nanoprobes for Gastric Computed Tomography Imaging. *Chin J Anal Chem* (2018) 46(10):1539–43. doi: 10.1016/S1872-2040(18)61116-8
38. Li NS, Chen L, Xiao ZX, Yang YQ, Ai KL. Progress in Detection of Biomarker of Ovarian Cancer: Lysophosphatidic Acid. *Chin J Anal Chem* (2020) 48 (12):1597–606. doi: 10.19756/j.issn.0253.3820.201339
39. Zhu S, Tian R, Antaris AL, Chen X, Dai H. Near-Infrared-II Molecular Dyes for Cancer Imaging and Surgery. *Adv Mater* (2019) 31(24):e1900321. doi: 10.1002/adma.201900321

Conflict of Interest: The authors declare that the research was conducted in the absence of any commercial or financial relationships that could be construed as a potential conflict of interest.

Publisher's Note: All claims expressed in this article are solely those of the authors and do not necessarily represent those of their affiliated organizations, or those of the publisher, the editors and the reviewers. Any product that may be evaluated in this article, or claim that may be made by its manufacturer, is not guaranteed or endorsed by the publisher.